

UNIVERSIDADE DE SÃO PAULO

INSTITUTO DE FÍSICA  
CAIXA POSTAL 20516  
01452-990 SÃO PAULO - SP  
BRASIL

# PUBLICAÇÕES

IFUSP/P-1103

SYNOPSIS 862132

**HADRONIZATION AND INELASTICITIES**

**F.O. Durães and F.S. Navarra**

Instituto de Física, Universidade de São Paulo

**G. Wilk**

Soltan Institut for Nuclear Studies, Nuclear Theory Department  
ul. Hoza 69, Warsaw, Poland

Março/1994

# HADRONIZATION AND INELASTICITIES

F.O. Durães and F.S. Navarra

Instituto de Física, Universidade de São Paulo  
C.P. 20516, 01452-990 São Paulo, SP, Brazil

and

G. Wilk

Soltan Institute for Nuclear Studies, Nuclear Theory Department  
ul. Hoża 69, Warsaw, Poland

## ABSTRACT

In this work we extend our previous analysis concerning the behavior of inelasticity at high energies and discuss the effects of the hadronization process on this quantity. We analyze the UA5 and UA7 data on rapidity distributions.

## 1 INTRODUCTION

The energy dependence of inelasticity is an important problem which is still subject of debate [1]–[4]. Generally speaking, inelasticity is the fraction of the total energy carried by the produced particles in a given collision. However in the literature one finds several possible ways to define it. We will be concerned with two of these definitions. In the first one, inelasticity is defined as

$$K_1 = \frac{M}{\sqrt{s}} \quad (1)$$

where  $\sqrt{s}$  is the total reaction energy in its center of mass frame and  $M$  is the mass of the system (fireball, string, etc.) which decays into the final produced particles. The second definition of  $K$  considered here is

$$K_2 = \frac{1}{\sqrt{s}} \sum_i \int dy \mu_i \frac{dn_i}{dy} \cosh y \quad (2)$$

where  $\mu_i = \sqrt{p_{T_i}^2 + m_i^2}$  is the transverse mass of produced particles of type  $i$  and  $\frac{dn_i}{dy}$  their measured rapidity distribution. These two definitions are, in principle, model independent, although the mass  $M$  might be difficult to evaluate in certain models.

The main difference between  $K_1$  and  $K_2$  is that, whereas the first one refers to partons, the second one refers to final observed hadrons.  $K_2$  implicitly includes the kinetic energy of the object of mass  $M$ .

From the experimental point of view  $K_2$  would be easy to measure. However errors on the measurements of fast (large  $y$ ) particles produce large uncertainties in the integral in (2) due to the  $\cosh y$  term. The solution of this problem would be to measure produced particles at very small angles, close to the beam. Unfortunately this is experimentally very difficult. However an important step in this direction was given by the CERN UA7 collaboration, which reported the measurement of the production cross section of neutral pions in a very forward region at  $\sqrt{s} = 630$  GeV. These data help not only in computing  $K_2$  but are in themselves important piece of experimental information and models should compare their predictions with UA5 [5] and UA7 [6] data simultaneously. So far such a comparison was only performed in refs. 2 and 4 where extremely simple models were considered.

From the theoretical point of view,  $K_1$  is a very interesting quantity because it can be easy to calculate and because it is the relevant quantity when studying the formation of dense systems (e.g. quark-gluon plasma).

In a recent paper [7] we have used the Interacting Gluon Model (IGM) [8] to study the energy dependence of  $K_1$ . We concluded that the introduction of a semihard component (minijets) in that model produces increasing inelasticities at the partonic level. In the present work we introduce a hadronization mechanism in the IGM, calculate the rapidity distributions of the produced particles, compare our results with the UA5 and UA7 data and finally calculate  $K_2$ . The purpose of this exercise is to verify whether the

hadronization process changes our previous conclusion. As it will be seen, we find out that, whereas some quantitative aspects, like the existence or not of Feynman Scaling [9, 10] in the fragmentation region and the numerical values of  $K_2$ , depend very strongly on details of the fragmentation process, the statement that minijets lead to increasing inelasticities remains valid.

## 2 HADRONIZATION IN THE IGM

### 2.1 General ideas of IGM

In the IGM a proton-proton collision is described as follows: during the collision the valence quarks in the protons fly through each other almost without interaction and form fast excited states called "Leading Jets" (L.J.) which will subsequently decay populating the "fragmentation region" with one leading baryon and a few hadrons. The gluon cloud, which surrounds the valence quarks and is the slow part of the proton, interacts strongly with the gluonic cloud in the other proton. There is a large amount of "stopping" and the formation of a gluonic cluster called "Central Fireball" (C.F.), which is the main source of secondary particles. This process is depicted in figure 1.

As extensively discussed in ref. [7, 8] and other previous publications, the fundamental quantity in the IGM is the function  $\chi(x, y)$  which gives the probability of depositing fractions  $x$  and  $y$  of the energy momenta of the incoming protons in the central region of reaction, by means of multiple gluon-gluon interactions in both soft and semihard regimes.

Given  $\chi(x, y)$  we can immediately write the inelasticity distribution and its complementary distribution, the leading jet momentum spectrum

$$\chi(K_1) = \int_0^1 dx \int_0^1 dy \delta(\sqrt{xy} - K_1) \chi(x, y) \theta(xy - K_{\min}^2) \quad (3)$$

$$f(x_L) = \int_0^1 dx \int_0^1 dy \delta(1 - x - x_L) \chi(x, y) \theta(xy - K_{\min}^2) \quad (4)$$

where  $K_1 = \sqrt{xy}$  and  $K_{\min}$  is the minimal inelasticity

$$K_{\min} = \frac{m_0}{\sqrt{s}} \quad (5)$$

which is defined by the mass  $m_0$  ( $= 350$  MeV) of the lightest possible produced state and  $\sqrt{s}$  is the invariant reaction energy.

In the past,  $x_L$  was identified with the leading particle fractional momentum. Here it is the momentum of the leading jet (L.J.) which contains the proton valence quarks and a few gluons. The leading jet decays into the leading particle and other fragments.

### 2.2 Hadronization of the Central Fireball

In order to calculate rapidity distributions and confront them with UA5 and UA7 data we must hadronize our Central Fireball, which has mass  $M = \sqrt{xy s}$  and our leading jet which has mass  $m_{LJ}$ . These two systems have a different nature. Whereas the former is rich in gluons, the latter is rich in quarks. This suggests that the hadronization mechanisms are different. In the lack of a better understanding of this hadronization phase we shall assume that the Central Fireball will decay like a fluid, i.e., each fireball with mass  $M$  will decay into particles which are distributed in rapidity according to  $\frac{dn_M}{dy}$  given by

$$\frac{dn_M}{dy} = \frac{\langle n \rangle_{ch}^{CF}}{\sqrt{\pi} L_M} \exp \left\{ -\frac{(y - y_M)^2}{L_M} \right\} \quad (6)$$

where

$$\langle n \rangle_{ch}^{CF} = a_1(M)^{a_2}, \quad L_M = a_3(M)^{a_4}, \quad y_M = \frac{1}{2} \ln \frac{x}{y} \quad (7)$$

and the final central rapidity distribution is given by

$$\frac{dn^{CF}}{dy} = \int_0^1 dx \int_0^1 dy \chi(x, y) \frac{dn_M}{dy}(x, y) \theta(xy - K_{\min}^2) \quad (8)$$

Expression (6) is the famous approximate one dimensional solution of Landau's hydrodynamical model. For thermalized systems this distribution would give a realistic description of the motion. Here, however, it is taken just as an empirical formula which describes data in an economical and successful way [11]. It depends on the parameters  $a_1, a_2, a_3$  and  $a_4$  which are energy independent and will be fixed later.

### 2.3 Hadronization of the Leading Jet

As was already mentioned before, the IGM is, in principle, not particularly suited for the fragmentation of L.J. - mainly because all our partons are regarded as massless. However, if we want to compare the IGM with more detailed data on particle production (and not only with inelasticity and leading particle spectra as was done in [7, 8]), we must include in it also the possibility of fragmentation of the L.J. In what follows the leading jet will be hadronized according to the simple independent fragmentation approach [12]. In order to perform the calculations we need to specify:

- (i) the momentum distributions of the valence quarks in the leading jet,
- (ii) the mass  $m$  of the leading jet and
- (iii) the momentum fraction of the leading jet taken away by the leading particle.

As for the momentum distribution of the valence quarks in the leading jet we assume it to be a gaussian centered around one third of the L.J. momentum with some width  $\sigma$ :

$$Q(x_i) = \frac{1}{\sqrt{\pi\sigma}} \exp \left\{ - \left( x_i - \frac{x_L}{3} \right)^2 / \sigma \right\} \quad (9)$$

The picture of "just going through and noninteracting" valence quarks used in the original IGM leads automatically to the massless L.J.'s,  $m_{L.J.} = 0$ . However, one can point out at least three mechanisms by which L.J. can acquire mass (and which were not

considered in the previous versions of the IGM). The mass  $m_{L.J.}$  is different from zero (and can be quite substantial) if the longitudinal momentum  $x_i$  of any  $i^{th}$  valence quark is small with respect to the longitudinal momentum of L.J.,  $x_L$ . This case corresponds to a situation where the  $i^{th}$  quark is retarded with respect to the others, stretching a string between itself and the other faster quarks. Another possibility is when the time-like virtuality of this quark,  $Q_i^2$ , is large, meaning that it is "overdressed" by gluons. Finally  $m_{L.J.}$  will be large if at least one of the quarks undergoes hard or semihard scattering on a gluon or a quark of the other proton and acquires transverse momentum  $k_T$ , [13]. As we do not control here any of the mechanisms mentioned we shall in what follows simply parametrize  $m_{L.J.}$  in the following way:

$$m_{L.J.} = \frac{m^H \sigma^H + m^S \sigma^S}{\sigma^H + \sigma^S} \quad (10)$$

where  $\sigma^S$  and  $\sigma^H$  are the integrated parton-parton cross sections in the soft and semihard regime respectively and depend on  $\sqrt{s}$  ( $m^H = \sqrt{3}p_{r_{min}}$  stands for the mass in the case of semihard scatterings where  $p_{r_{min}} = 2.3$  GeV is the minimum transverse momentum acquired by a parton during a semihard collision whereas  $m^S = \sqrt{3}m_0 = \sqrt{3} \cdot 0.35$  GeV is the mass when there are only soft interactions). Once we know the mass of the leading jet, using experimental information coming from  $e^+e^-$  studies [14], we can calculate its average charged multiplicity

$$\langle n \rangle_{ch}^{L.J.} = 2.18 (m_{L.J.})^{1/4} \quad (11)$$

As for the last point we shall assume for simplicity that the leading particle takes always half of the leading jet momentum, i.e.  $x_{LP} = x_L/2$ . This approximation was also done by Gaisser and Stanev [15]. (As a consequence, when applying eqs. (12) and (14) below to the description of hadronic rapidity distributions, especially to the UA7 data,

we have to replace  $x_L$  by  $x_L/2$  in the argument of the delta function and we have also to subtract the baryon mass in (11):  $m_{L,J} \rightarrow m_{L,J} - m_p$  ( $m_p = 0.938$  GeV).

Following the independent fragmentation scheme a quark with momentum  $x_i$  will fragment into hadrons of momentum  $x_h$  according to the fragmentation functions  $D_q^h(z)$  where  $z = x_h/x_i$ . The hadron momentum distribution normalized to  $\langle n \rangle_{ch}^{L,J}$ , will then be given by the convolution

$$\frac{dn}{dx_h} = \langle n \rangle_{ch}^{L,J} \int_{x_h}^1 dx_L f(x_L) \int \prod_{i=1}^3 dx_i \sum_{i=1}^3 Q(x_i) D_q^h\left(\frac{x_h}{x_i}\right) \delta\left(x_L - \sum_{i=1}^3 x_i\right) \quad (12)$$

From the above expression we obtain the rapidity distribution by changing variables to

$$x_h = \frac{2\mu}{\sqrt{s}} \sinh y,$$

where  $\mu = ((p_T)^2 + m_h^2)^{1/2}$  is the hadron transverse mass and  $\langle p_T \rangle$  is the average transverse momentum of the produced hadron which is a function of the rapidity and is given here by the following formula used by the UA7 collaboration [6]:

$$\langle p_T \rangle = \langle p_{T0} \rangle \left\{ 1 - \exp[a(y_{\text{beam}} - y - y_0)^b] \right\} \quad (13)$$

with  $\langle p_{T0} \rangle = 0.35$  GeV,  $y_{\text{beam}} = \ln(\sqrt{s}/m)$ ,  $y_0 = 1.7$ ,  $a = -0.21$ ,  $b = 2.0$  and  $m = 0.938$  GeV.

The final fragmentation rapidity distribution is given by

$$\frac{dn^{L,J}}{dy} = \frac{dn}{dx_h} \frac{dx_h}{dy} \quad (14)$$

For simplicity we assume that  $D_u^h = D_d^h = D_s^h = D_{\bar{u}}^h = D_{\bar{d}}^h = D_{\bar{s}}^h$  which is [12]

$$D_u^h(z) = \beta \left[ \frac{1}{2} + \beta \left( \frac{1}{z} - 1 \right) \right] (d+1)(1-z)^d \quad (15)$$

with  $\beta = 0.4$  and  $d = 2$ . The fragmentation function  $D(z)$  diverges like  $1/z$  at  $z \rightarrow 0$  or equivalently  $x_h \rightarrow 0$ . This behavior causes problems in the calculation of the momentum distributions. We have regularized it by the replacement

$$\frac{1}{z} = \frac{x_i}{x_h} \rightarrow \frac{x_i}{\sqrt{x_h^2 + x_0^2}}$$

where  $x_0$  is the fractional momentum of the lightest produced hadron,  $x_0 \cong m_0/\sqrt{s}$ .

### 3 RESULTS AND DISCUSSION

Using eqs. (8) and (14) we write the total rapidity distribution as

$$\frac{dn}{dy} = \frac{dn^{CF}}{dy} + \frac{dn^{L,J}}{dy} \quad (16)$$

The pseudorapidity distribution is obtained from (16) by a simple change of variables,

$$p_T \sinh \eta = \mu \sinh y:$$

$$\frac{dn}{d\eta} = \frac{dn}{dy}(\eta) \frac{dy}{d\eta}(\eta) = \frac{dn}{dy}(\eta) \frac{\langle p_T \rangle}{\mu} \frac{\cosh \eta}{\cosh y(\eta)} \quad (17)$$

In figure 2 we show pseudorapidity distributions calculated with (17) and compared to UA5 data at different energies [5] and CDF [16] data at  $\sqrt{s} = 1800$  GeV. The parameters used in this fit are  $a_1 = 3.70$ ,  $a_2 = 0.76$ ,  $a_3 = 2.25$  and  $a_4 = 0.75$ ;  $\sigma$ , appearing in (9) was chosen to be 1.0. As it can be seen the agreement is quite good. Figure 3 shows a comparison between our calculations and UA7 data on fast  $\pi^0$ 's. Again reasonable agreement is found. Figure 4 shows the relative contributions of the central and fragmentation regions separately and the sum of them. We first notice that the central region gives a significant contribution to the large rapidity tail of the total distribution and also that the fragmentation region gives some non-negligible contribution to the low rapidity part of the total distribution. We also observe that at increasing energies the contribution coming from the central fireball becomes more and more important. This is so because the multiplicity coming from the fragmentation region (which determines the normalization of  $\frac{dn^{L,J}}{dy}$ ) depends on  $m_{L,J}$ , which grows very slowly with energy. Figure 5a shows the average charged multiplicity and 5b) the central pseudorapidity density, both as a function of the reaction energy  $\sqrt{s}$ . Also shown are the relative contributions

from the central and fragmentation regions and the corresponding experimental data. As before we find good agreement with data and the increasing importance of the central region contribution. For the sake of comparison with other models based both on soft and semihard dynamics, we show in figure 6 our results for the multiplicity (figure 6a) and central rapidity density (figure 6b) together with the results of HIJING [17] for the same quantities. Both models fit the data but differ significantly when one switches off the semihard (minijet) contribution. Whereas in HIJING Feynman Scaling violation in central region (the growth of  $\left. \frac{dn}{d\eta} \right|_{\eta=0}$  with  $\sqrt{s}$ ) is entirely due to the minijets, in the IGM this behavior is partly due to soft interactions, there being only a quantitative difference when minijets are included.

As it was pointed out in ref. [5] when all UA5 pseudorapidity distributions are plotted in the beam frame, i.e. as a function of  $\eta - y_{\text{beam}}$  (where  $y_{\text{beam}} = \ln \sqrt{s}/m_p$ ;  $m_p =$  proton mass) we observe that all the tails of these curves nearly coincide. This means that the pseudorapidity distribution tails have all the same aspect and are energy independent. Further evidence for approximate Feynman Scaling (FS) in the forward region can be found in the UA7 analysis.

In figure 7 we present the same plot shown in ref. [5] with the inclusion of one more energy ( $\sqrt{s} = 1800$  GeV). These curves exhibit a small degree of scaling violation, consistent with experimental data.

From this analysis we conclude that our model is consistent with all rapidity distribution data and both theory and experiment are consistent with approximate Feynman Scaling at large rapidities.

We turn now our attention to  $K_2$ . With the rapidity distributions (17) we can immediately calculate  $K_2$  using the definition (2). Since we have been dealing with charged particles and almost all of them are pions, we replace the sum in eq. (2) by the factor  $\frac{3}{2}$  to account for neutral pions.

In figure 8 we plot  $K_2$  (full lines) and  $K_1$  (dashed lines, calculated in ref. [7]) as a function of  $\sqrt{s}$ . The lower curves show the results when minijets are switched off and only soft interactions take place. The upper curves show the effect of including minijets. At this point two comments are in order. First, the fact that  $K_2$  grows so fast, almost approaching 1.0 at 2 TeV, is a consequence of our fit of the rapidity distributions. At higher energies, these distributions are dominated by the CF component, whose width is essentially given by  $L_M (= a_3 \sqrt{xys}^{a_4})$ . The value found here for  $a_4$ , although good enough for fitting the data, is probably too large. Second, up to values around 1 TeV, the lower full line lies below the dashed line. This unexpected behavior is a consequence of our fits and comes from the tails of the theoretical rapidity distributions at  $\sqrt{s} = 53, 200$  and 540 GeV, which, as it can be seen in figure 2, lie below data. These two features could be changed just by fitting data again and finding different values for the parameters. Although possible, in view of the uncertainties of higher energies data at large rapidities (which are crucial in determining  $K_2$ ), we believe that this exercise would not be very interesting. We have checked that with different choices of the momentum fraction of the leading jet taken away by the leading particle ( $x_{LP} = 0.1 x_L, 0.5 x_L$  and  $0.9 x_L$ ) we can still fit the rapidity distribution data and we obtain qualitatively the same result in what concerns the energy dependence of our inelasticities. The solid lines in figure 8 become areas but we still have increasing upper (with minijets) areas and decreasing lower (without minijets) areas.

Finally we remember that our hadronization model is very simple. Improvements on this model or the use of another hadronization scheme would lead to quantitative changes in  $K_2$ . We believe that the hadronization procedure used here is neither the best nor the most detailed one, but it leads to reasonable, non-exotic results and thus it can be regarded as representative of the good and complicated models.

Having in mind the limitations of our calculations and not sticking to precise numbers, one clear conclusion emerges from figure 8: minijets lead to inelasticities increasing with energy and hadronization does not change this trend. Note also that there is a marked difference between both inelasticities used here,  $K_1$  and  $K_2$ , and the growth of  $K_1$  is only moderate. It is therefore important to specify precisely which type of inelasticity one has in mind in discussing its energy dependence and comparing it with data [1].

#### ACKNOWLEDGEMENTS

This work was supported partially by FAPESP, by CNPq and by the Polish State Committee for Scientific Research Grant No. 2 0423 91 01 (GW). We are deeply indebted to C.Y. Wong for valuable discussions.

#### References

- [1] Y.M. Shabelski et al., *J. Phys.* **G18** (1992) 1281 and references therein.
- [2] D. Linkai and Z. Qingqi, *Phys. Lett.* **B297** (1992) 201
- [3] M.T. Nazirov and P.A. Usik, *J. Phys.* **G18** (1992) L7
- [4] J. Dias de Deus and A.B. Padua, *Phys. Lett.* **B315** (1993) 188; A. Ohsawa and K. Sawayanagi, *Phys. Rev.* **D45** (1992) 3128
- [5] C. Geich-Gimbel, *Int. Jour. Mod. Phys.* **A4** (1989) 1527
- [6] E. Pare et al., *Phys. Lett.* **B242** (1990) 531
- [7] F.O. Durães, F.S. Navarra and G. Wilk, *Phys. Rev.* **D47** (1993) 3049

- [8] G.N.Fowler et al., *Phys. Rev.* **C40** (1989) 1219 and references therein (cf. also R. Weiner, G. Wilk and W. Włodarczyk, Soltan Institute for Nuclear Studies Report, SINS-2153/VIII/1993).
- [9] J. Wdowczyk and A.W. Wolfendale, *J. Phys.* **G13** (1987) 411; *J. Phys.* **G10** (1984) 257
- [10] R. Feynman, *Phys. Rev. Lett.* **23** (1969) 1415
- [11] D.K. Srivastava, J. Alam and B. Sinha, *Phys. Lett.* **B298** (1993) 257; Y. Hama and F.S. Navarra, *Z. Phys.* **C26** (1984) 465
- [12] R.D. Field, Applications of Perturbative QCD, *Frontiers in Physics*, Vol. 77, 1989; R.D. Field and R.P. Feynman, *Phys. Rev.* **D15** (1977) 2590; *Nucl. Phys.* **B138**, (1978) 1; R.P. Feynman, R.D. Field and G.C. Fox, *Phys. Rev.* **D18** (1978) 3320.
- [13] All this follows from the approximate estimation of the mass of leading jet:  $m_{L.L.}^2 = x_L \sum_{i=1}^3 \frac{Q_i^2 + k_{Ti}^2}{x_i}$  which is valid for  $Q_i \ll x_i \sqrt{s}/2$  and  $k_{Ti} \ll \sqrt{s}/2$ ; see also M.T. Nazirov, *Mod. Phys. Lett.* **A20** (1990) 1587.
- [14] X.N. Wang, *Phys. Rev.* **D43** (1991) 104 and references therein.
- [15] T.K. Gaisser and T. Stanev, *Phys. Lett.* **219** (1989) 375
- [16] F. Abe et al., *Phys. Rev.* **D41** (1990) 2330
- [17] X.N. Wang and M. Gyulassy, *Phys. Rev.* **D45** (1992) 844

## FIGURE CAPTIONS

Figure 1: Illustration of a proton-proton collision: fractions  $x$  and  $y$  of the incoming protons momenta form the central fireball (CF) and fractions  $1-x$ ,  $1-y$  are carried by the leading jets (L.J.).

Figure 2: Pseudorapidity distributions measured at the central rapidity region. Data are from the UA5 collaboration [5] at different energies and from CDF collaboration [16] at  $\sqrt{s} = 1800$  GeV. Full lines show the IGM results.

Figure 3: Rapidity distribution of neutral pions measured at the fragmentation (large rapidities) region. Data are from the UA7 collaboration [6] and the full line is the IGM result.

Figure 4: Pseudorapidity distribution at  $\sqrt{s} = 540$  and 53 GeV. Dashed and dash-dotted lines represent the individual contributions of the central fireball and the leading jet respectively.

Figure 5: a) Average charged multiplicities as a function of the reaction energy. Squares and circles are experimental data. Dashed, dash-dotted and full lines show the central fireball contribution, the leading jet contribution and the total IGM result respectively.

b) The same as a) for the central pseudorapidity distribution  $\left. \frac{dn}{d\eta} \right|_{\eta=0}$ .

Figure 6: a) Average charged multiplicities as a function of the reaction energy. Squares and circles are experimental data. Full lines show the IGM results with and without the semihard contribution (lower curve). Dashed lines show the same quantities calculated with HIJING.

b) The same as a) for the central pseudorapidity distribution  $\left. \frac{dn}{d\eta} \right|_{\eta=0}$ .

Figure 7: IGM results of figure 2 plotted in the beam frame, i.e. as a function of  $\eta - \eta_{\text{beam}}$ .

Figure 8: Inelasticities  $K_1$  (dashed lines) and  $K_2$  (solid lines) with minijets (upper curves) and without minijets (lower curves) as a function of the reaction energy.



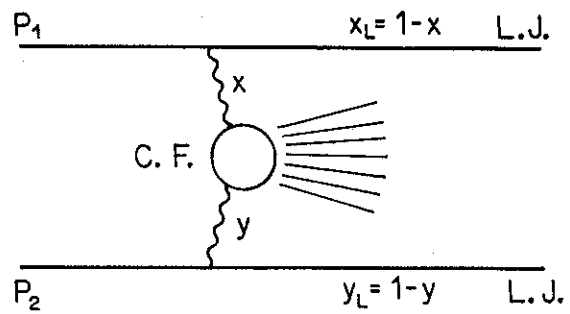


Figure 1

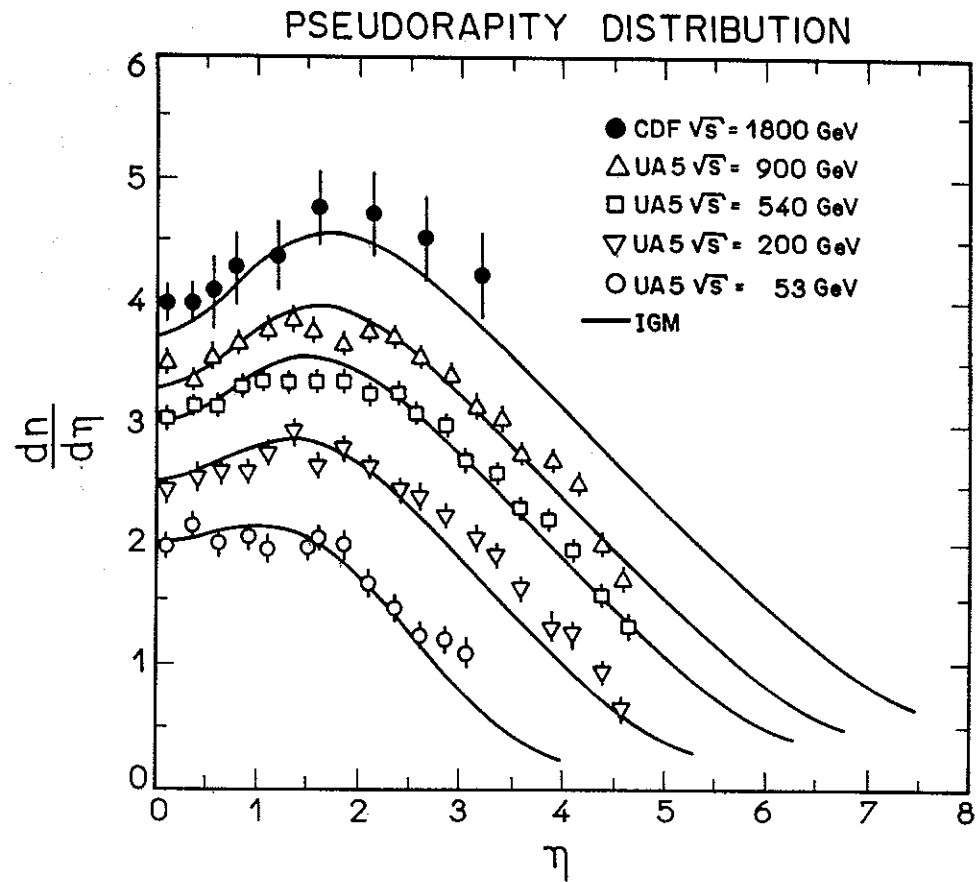


Figure 2

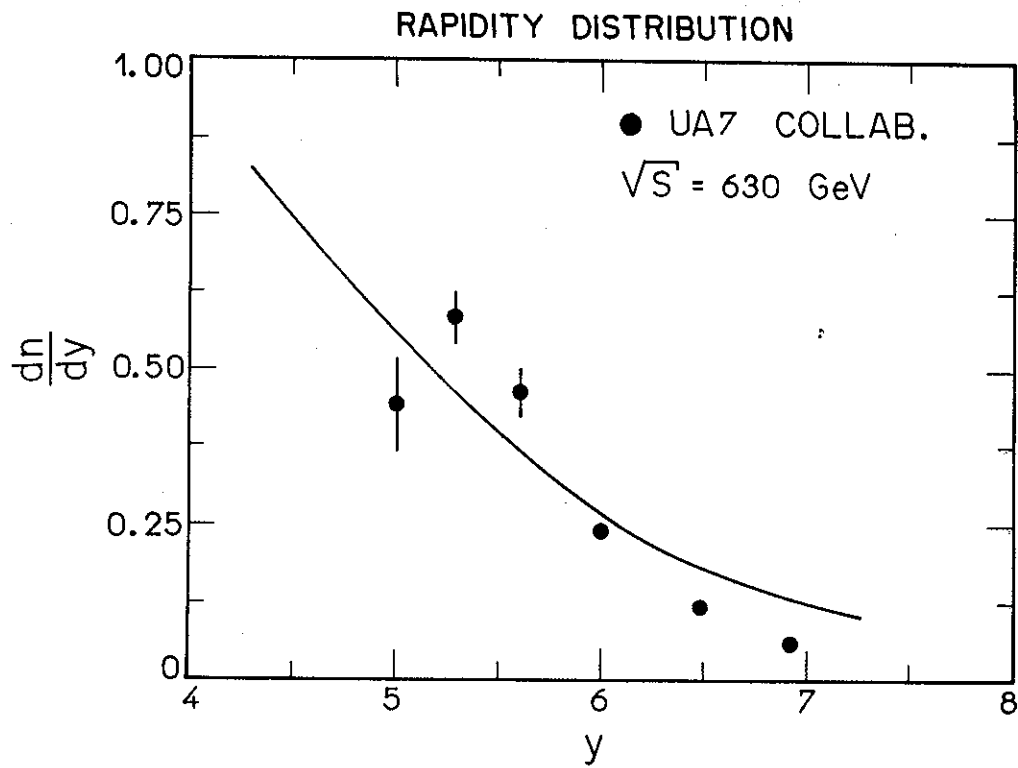


Figure 3

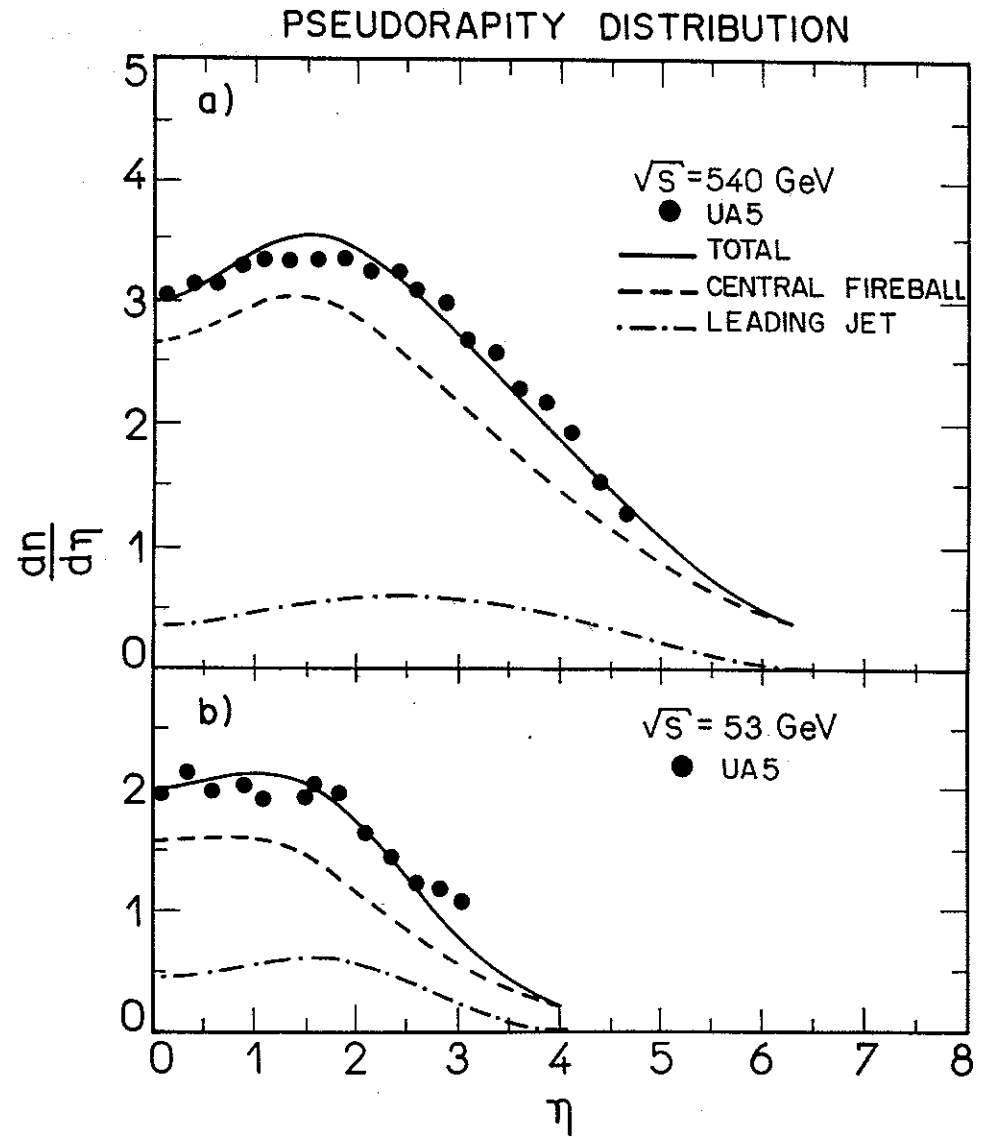


Figure 4

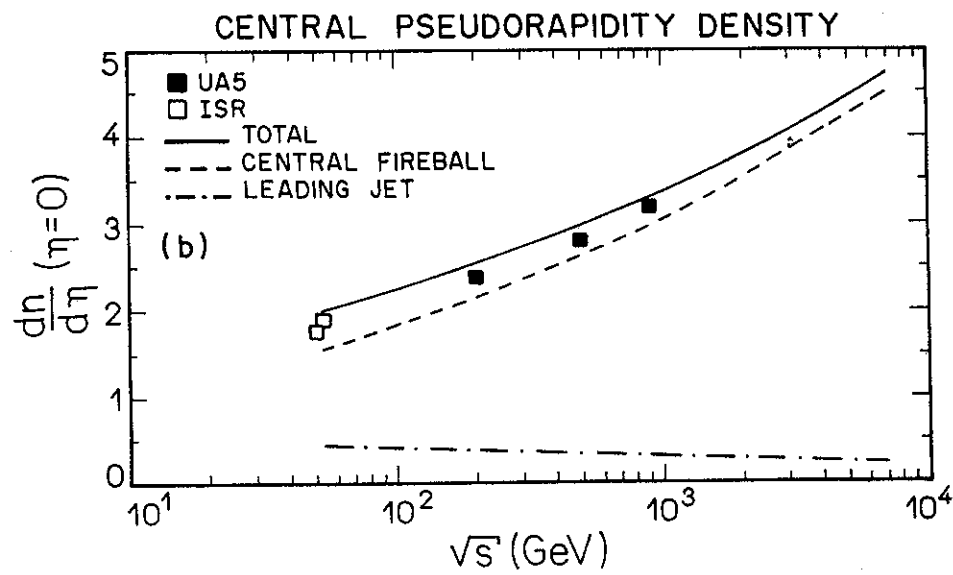
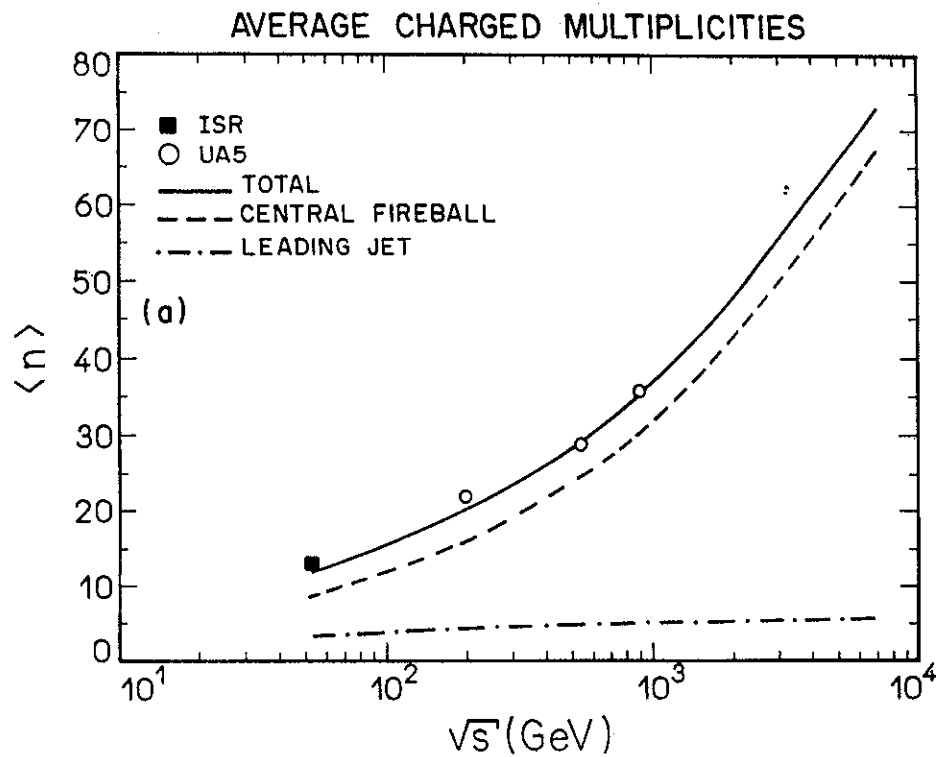


Figure 5

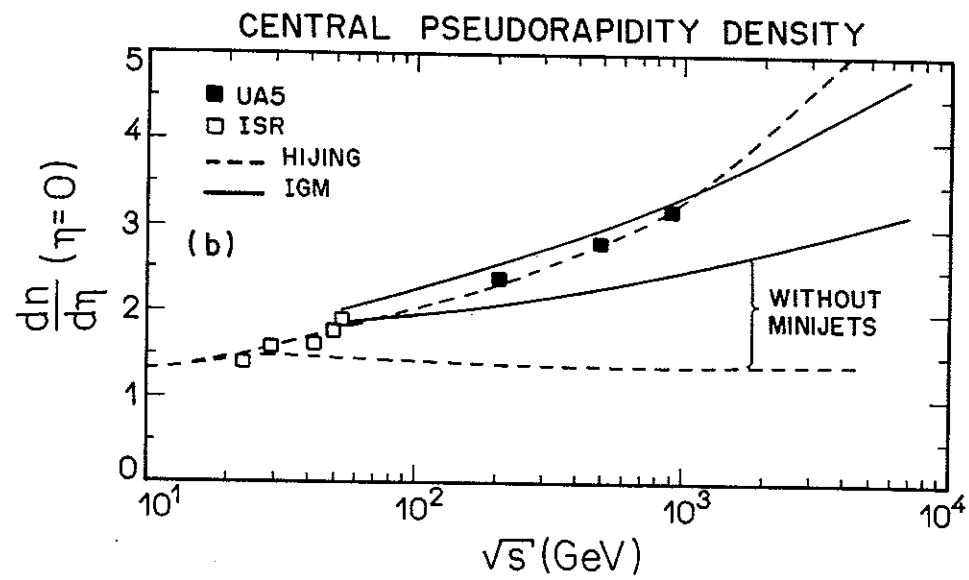
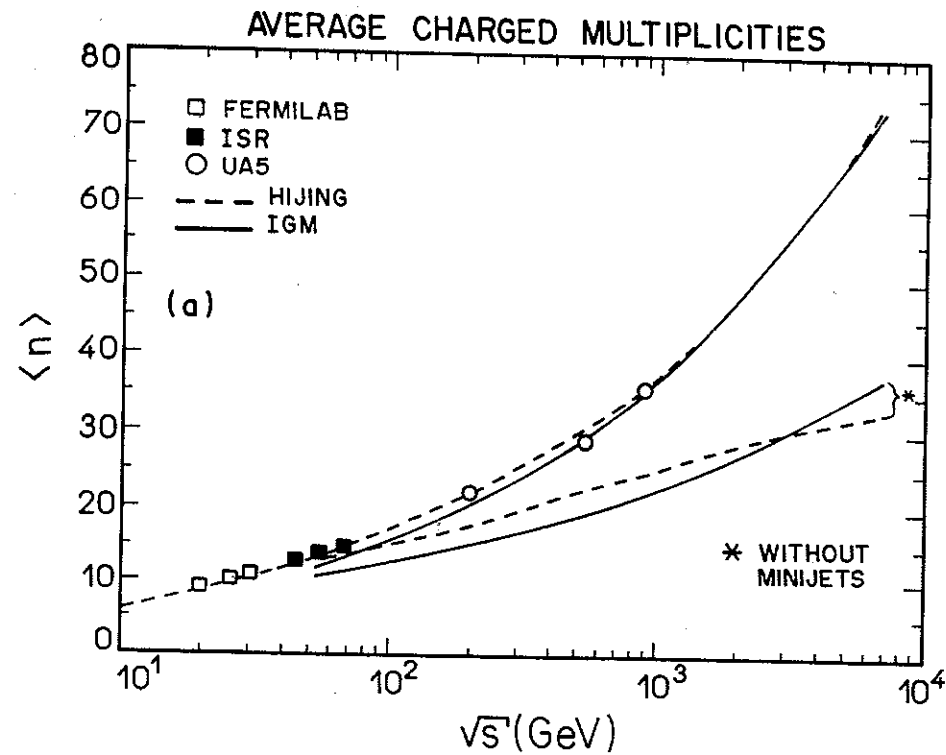


Figure 6

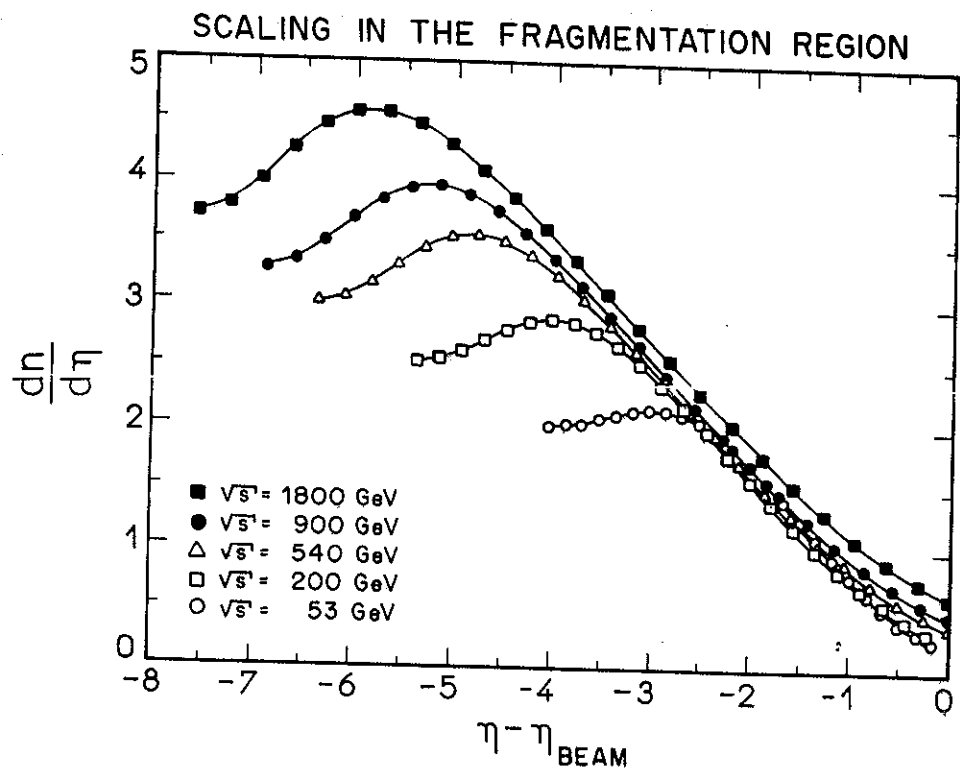


Figure 7

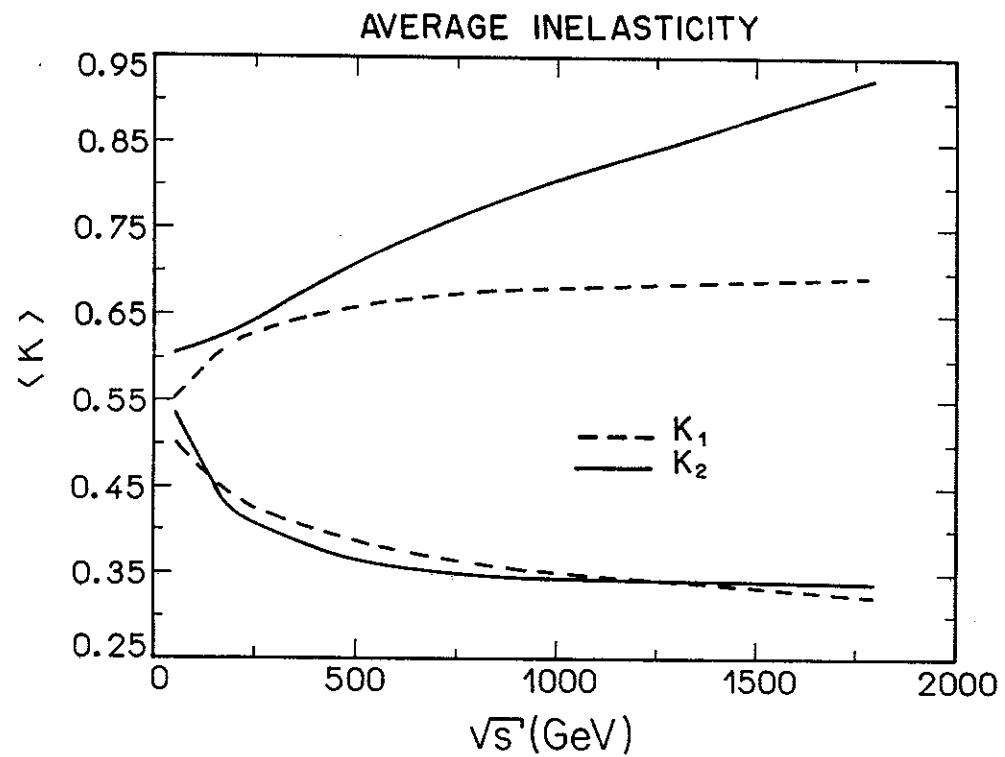


Figure 8